◆ Human Brain Mapping 32:341–357 (2011) ◆

Functional Localization in the Human Brain: Gradient-Echo, Spin-Echo, and Arterial Spin-Labeling fMRI Compared with Neuronavigated TMS

Svenja Diekhoff,[1] Kamil Uludağ,[2] Roland Sparing,[3] Marc Tittgemeyer,[1] Mustafa Cavuşoğlu,[2] D. Yves von Cramon,[1] and Christian Grefkes[1,3]*

[1]*Max Planck Institute for Neurological Research, Cologne, Germany*
[2]*High-Field Magnetic Resonance Center, Max Planck Institute for Biological Cybernetics, Tübingen, Germany*
[3]*Department of Neurology, University of Cologne, Cologne, Germany*

Abstract: A spatial mismatch of up to 14 mm between optimal transcranial magnetic stimulation (TMS) site and functional magnetic resonance imaging (fMRI) signal has consistently been reported for the primary motor cortex. The underlying cause might be the effect of magnetic susceptibility around large draining veins in Gradient-Echo blood oxygenation level-dependent (GRE-BOLD) fMRI. We tested whether alternative fMRI sequences such as Spin-Echo (SE-BOLD) or Arterial Spin-Labeling (ASL) assessing cerebral blood flow (ASL-CBF) may localize neural activity closer to optimal TMS positions and primary motor cortex than GRE-BOLD. GRE-BOLD, SE-BOLD, and ASL-CBF signal changes during right thumb abductions were obtained from 15 healthy subjects at 3 Tesla. In 12 subjects, tissue at fMRI maxima was stimulated with neuronavigated TMS to compare motor-evoked potentials (MEPs). Euclidean distances between the fMRI center-of-gravity (CoG) and the TMS motor mapping CoG were calculated. Highest SE-BOLD and ASL-CBF signal changes were located in the anterior wall of the central sulcus [Brodmann Area 4 (BA4)], whereas highest GRE-BOLD signal changes were significantly closer to the gyral surface. TMS at GRE-BOLD maxima resulted in higher MEPs which might be attributed to significantly higher electric field strengths. TMS-CoGs were significantly anterior to fMRI-CoGs but distances were not statistically different across sequences. Our findings imply that spatial differences between fMRI and TMS are unlikely to be caused by spatial unspecificity of GRE-BOLD fMRI but might be attributed to other factors, e.g., interactions between TMS-induced electric field and neural tissue. Differences between techniques should be kept in mind when using fMRI coordinates as TMS (intervention) targets. *Hum Brain Mapp 32:341–357, 2011.* © 2010 Wiley-Liss, Inc.

Key words: perfusion; CBF; BOLD; GRE; SE; ASL; spatial; transcranial magnetic stimulation; functional magnetic resonance imaging; motor mapping

Additional Supporting Information may be found in the online version of this article.

*Correspondence to: Christian Grefkes, Neuromodulation & Neurorehabilitation, Max Planck Institute for Neurological Research, Gleueler Str. 50, Köln 50931, Germany.
E-mail: christian.grefkes@nf.mpg.de

Received for publication 21 September 2009; Revised 25 December 2009; Accepted 15 January 2010

DOI: 10.1002/hbm.21024
Published online 9 June 2010 in Wiley Online Library (wileyonlinelibrary.com).

INTRODUCTION

Gradient-Echo (GRE) echo planar imaging (EPI) is by far the most widely used technique for functional magnetic resonance imaging (fMRI) due to high data acquisition efficiency and high sensitivity to T_2* effects [Liu and Brown, 2007]. The underlying blood oxygenation level-dependent (BOLD) contrast relies on alterations of local magnetic susceptibility mainly caused by changes in deoxyhemoglobin level reflecting the increased metabolic demands due to enhanced neural activity (for a recent review see: Logothetis [2008]). However, such changes do not only occur in small blood vessels in brain parenchyma (e.g., gray matter) but also in large draining veins [Buxton et al. 1998]. GRE-BOLD signal has been shown to be sensitive to both T_2* changes in parenchyma as well as in and around large draining veins [Boxerman et al., 1995; Frahm et al., 1994; Uludag et al., 2009] and hence GRE-BOLD signal changes may show a spatial displacement from actual neuronal activities, reducing the specificity for functional localization. Spin-Echo (SE) EPI is an alternative BOLD sequence which is sensitive to T_2 and has been suggested to be more accurate in functional localization at higher field strengths, i.e., from 3 Tesla (T) upwards [Duong et al., 2002; Lee et al., 2002; Thulborn et al., 1997; for review see: Norris, 2003; Uludag et al., 2009]. Decreased sensitivity of SE-BOLD for macrovasculature is achieved by an additional 180° refocusing pulse after half echo time refocusing static dephasing effects caused by local field inhomogenities around large vessels [Ye et al., 2009]. Along with SE-BOLD, Arterial Spin-Labeling (ASL) is an attractive alternative to GRE-BOLD. ASL allows measuring both, cerebral blood flow (CBF) as well as BOLD signal simultaneously. The signal type depends on the contrast calculated in the subsequent analysis, i.e., the BOLD contrast is the standard "activation vs. baseline" contrast, whereas the ASL-CBF contrast is the interaction between ASL-CBF time series (created by calculating control—tag differences) and the "activation vs. baseline" contrast. The ASL signal related to CBF (ASL-CBF) arises from magnetically labeled (i.e., tagged) arterial blood that has passed through the capillary walls into the tissue or is still located within capillaries [Silva et al., 1997]. A number of studies demonstrated that ASL-CBF is well co-localized with neuronal activity [Duong et al., 2000; Luh et al., 2000; Tjandra et al., 2005; Zappe et al., 2008; for reviews see: Liu and Brown, 2007; Silva, 2005].

Spatial accuracy of fMRI is especially important for fMRI informed (i.e., stereotaxically neuronavigated) transcranial magnetic stimulation (TMS). TMS is a well-established tool in neurosciences allowing noninvasive focal brain stimulation via externally applied magnetic fields [Barker et al., 1985]. Within the last decade, neuronavigation systems emerged allowing precise online monitoring of coil positions with reference to underlying brain structures and their functional properties assessed with anatomical or functional MRI, respectively. The potential of TMS in combination with fMRI is regarded to be high, especially for identification of TMS targets in the "virtual lesion" approach or in therapeutical intervention studies [Walsh and Cowey, 2000].

Several studies have already investigated the spatial congruence between positions yielding highest TMS effects, i.e., motor-evoked potentials (MEP), and positions with highest neural activity, i.e., highest statistical *t*-values, during hand movements measured by neuroimaging techniques such as positron emission tomography (PET) [Classen et al., 1998; Wassermann et al., 1996] or fMRI [Bastings et al., 1998; Boroojerdi et al., 1999; Herwig et al., 2002; Krings et al., 1997; Lotze et al., 2003; Sparing et al., 2008; Terao et al., 1998]. All studies reported good gross spatial correspondence between TMS and neuroimaging techniques as both techniques localized neural activity during hand movements within the precentral gyrus. However, if mean Euclidean distances between optimal TMS positions and highest neuroimaging signal were reported, they were often relatively large, i.e., 13 (±8.8) mm for ^{15}O PET (four subjects; Wassermann [1998]), 9.8 mm (eight subjects; Herwig et al. [2002]) and 13.9 mm (five subjects; Lotze et al. [2003]) for fMRI. Only one study reported relatively short mean 3D distances, i.e., 3.3 ± 0.8 mm (five subjects; Terao et al. [1998]) between TMS and fMRI. Hence, although all studies reported fairly good correspondence between TMS and fMRI, a considerably large residual mismatch has consistently been demonstrated rising the question whether these differences can be solely attributed to technical issues (e.g., coregistration inaccuracy or spatial unspecificity of fMRI signal) or if both techniques probe different underlying (neuronal) processes. Although relatively small sample sizes (in the majority of studies 4–5 subjects) and technical limitations due to unavailability of neuronagivated stimulation systems [Lotze et al., 2003; Terao et al., 1998; Wassermann, 1998] might have influenced spatial accuracy, the exact cause of the spatial mismatch remains unknown.

In the present study, we aimed to investigate whether displacements between TMS and fMRI might rely on the fMRI sequence used. All studies mentioned above used GRE-BOLD at 1.5 T (except for Krings et al. [1997] who used SE-BOLD at 1.5 T). Thus, all studies employed fMRI sequences that are susceptible to shifts towards large vessels at low field strengths. Hence, the observed mismatch between fMRI and TMS might, at least partially, be explained by inaccurate localization of motor hand area by the fMRI sequences used.

We, therefore, hypothesized that at 3 T, SE-BOLD and ASL-CBF may provide more accurate information in terms of functional localization of the motor hand area than GRE-BOLD. In particular, we aimed to test the hypothesis that spatial differences are functionally relevant by stimulating brain tissue at fMRI peak voxel coordinates with single-pulse neuronavigated TMS. Finally, we aimed to answer the question whether the spatially more accurate

fMRI sequences better match with optimal TMS sites for evoking highest motor responses.

METHODS

Subjects

MRI measurements were performed on 15 healthy subjects (eight males; 21–31 years old; mean age 24.9 ± 2.7). Fourteen subjects were right-handed and one subject was left-handed according to the Edinburgh Handedness Inventory [Oldfield, 1971]. We did not exclude left-handers as we did not expect that handedness impacts on spatial localization accuracy of fMRI sequences. Twelve subjects participated in a subsequent TMS session (seven males; 23–31 years old; mean age 25.1 ± 2.7; all right-handed). None of the subjects had any history of medical or psychiatric disease or contraindication to TMS [Wassermann, 1998]. All subjects gave informed written consent to participate in this study, which was approved by the ethics committee of the Medical Faculty, University of Cologne, Germany (file-no 08-062). All experiments conformed to the Declaration of Helsinki, sixth revision, 2008.

fMRI Motor Paradigm

Subjects were asked to perform visually paced rhythmic right thumb abductions at a frequency of 1.55 Hz. The movement frequency was paced by a red blinking circle on white background presented on a shielded TFT screen at the rear end of the MR scanner visible via a mirror mounted on the MR headcoil. Blocks of thumb movements (20 s) were separated by resting baselines (40 s plus 0–6 s jitter) in which a black screen instructed the subjects to rest still until the next block of movements commenced. One fMRI session consisted of 10 cycles of baseline and movement blocks and lasted approximately 11 min. Each subject underwent three fMRI sessions, i.e., one for each fMRI sequence. The order of fMRI sequences was counterbalanced across subjects. Prior to scanning, subjects were trained until a stable performance was reached, which was monitored by visual inspection.

fMRI Data Acquisition

MR images were acquired on a 3 T Siemens MAGNETOM Trio TIM scanner. High-resolution anatomical T_1-weighted images were acquired using a 3D MP-RAGE (magnetization-prepared, rapid acquisition gradient echo) sequence with the following imaging parameters: Time of Repetition (TR) = 2000 ms, Echo Time (TE) = 3.25 ms, Field of View (FOV) = 256 mm, 176 sagittal slices, slice thickness = 1 mm, in-plane resolution = 1 × 1 mm^2, flip angle = 9°. Although CBF and BOLD signal changes can be measured simultaneously using ASL, this approach has been shown to result in a reduction of the BOLD signal in the order of 15% compared to conventional BOLD measurements [Luh et al., 2000]. Hence, a separate GRE-BOLD session was conducted in the present study to ensure that each fMRI measurement was conducted under optimal conditions. Altogether, we employed three different fMRI sequences: (i) GRE-BOLD EPI sequence with the following parameters: TR = 2200 ms, TE = 30 ms, FOV = 192 mm, 15 axial slices, slice thickness = 3 mm, in-plane resolution = 3 × 3 mm^2, distance factor = 10%, flip angle = 90°, (ii) SE-BOLD EPI sequence with identical imaging parameters except for a longer TE of 80 ms, and (iii) PICORE-Q2TIPS (quantitative imaging of perfusion using a single subtraction with thin slice TI_1 periodic saturation—proximal inversion with a control for off-resonance effects) ASL-CBF sequence [Luh et al., 1999] using a Frequency Offset Corrected Inversion pulse for inversion with the following parameters: TI_1 & equals; 700 ms, TI_{1s} = 900 ms, and TI_2 = 1400 ms, TR = 2200 ms, TE = 30 ms, FOV = 192 mm, 15 axial slices, slice thickness = 3 mm, in-plane resolution = 3 × 3 mm^2, distance factor = 10%, flip angle = 90°. The tag was 10 cm in width positioned at a 1 cm gap inferior to the imaging slices. Two presaturation pulses were applied in the imaging planes immediately before the inversion tag to minimize the impact of the static tissue. A 20-mm thick saturation slab was repeatedly applied for the bolus cutoff [Cavusoglu et al., 2009]. Images were acquired sequentially in ascending direction using a single-shot EPI technique. Slices covered a region extending from the body of the corpus callosum to the top of the parietofrontal vertex, thereby ensuring full coverage of the primary motor cortex along the central sulcus. Each fMRI session consisted of 310 EPI volumes including four "dummy" scans ensuring a steady-state in T_1 tissue contrast. 10 wholebrain EPI volumes (35 slices) were additionally acquired to improve the coregistration with the anatomical T_1 volume in data preprocessing (see below).

Analysis of Individual fMRI Data

For ASL sessions, ASL-CBF time series were created by calculating control-tag difference images (resulting in a total of 153 substraction images) using surround subtraction (i.e., computing the difference between each image and the average of its two nearest neighbors), thereby reducing BOLD signal contamination of the ASL-CBF time course (see Cavusoglu et al. [2009] for details). For image preprocessing and statistical analysis of GRE-BOLD, SE-BOLD, and ASL-CBF data, we used FEAT (FMRI Expert Analysis Tool) Version 5.98, part of FSL (FMRIB's Software Library, www.fmrib.ox.ac.uk/fsl). The following prestatistics processing was applied: motion correction using MCFLIRT [Jenkinson et al., 2002], nonbrain removal using Brain Extraction Tool (BET) [Smith, 2002], and spatial smoothing using a Gaussian kernel of 4-mm full-width half maximum (FWHM). Time-series statistical analysis was carried out using FILM (FMRIB's Improved Linear Model) with local autocorrelation correction [Woolrich

et al., 2001] and a high-pass filter of 1/60 Hz to remove low frequency drifts. Head motion parameters were included as covariates into the model. Z (Gaussianized T/F) statistic images were thresholded using a voxel-wise corrected significance threshold of $P < 0.001$ [Forman et al., 1995; Friston et al., 1994; Worsley et al., 1992]. ASL-CBF provided much weaker signal intensities than BOLD signal and thus, no correction for multiple comparisons was applied for the identification of peak voxel coordinates ($P < 0.001$, uncorrected). Coregistration to high-resolution images was carried out using FLIRT [Jenkinson et al., 2001, 2002].

Identification of fMRI Peak Voxel

The voxel with the highest statistical *t*-value located within the precentral gyrus near or at the hand knob was identified for each of the three fMRI sessions per subject. The hand knob is shaped like an omega or epsilon in the axial plane and hook-shaped in the sagittal plane, and has been shown to constitute a reliable anatomical landmark for the motor hand area [Yousry et al., 1997]. In two subjects no significant voxel could be observed in the precentral gyrus for the SE-BOLD session after correcting for multiple comparisons, and thus no correction was applied for identification of the peak voxel in these subjects ($P < 0.001$, uncorrected).

Identification of fMRI CoGs

While the peak voxel represents the site of maximal regional activity, the center-of-gravity (CoG) of an fMRI activation cluster considers the spatial distribution of activity in the pericentral region and hence might be less prone to a spatial shift towards large veins which usually produce high levels of activation [Luh et al., 2000]. Therefore, CoGs were computed for each of the three fMRI sessions per subject. In contrast to peak voxel coordinates, CoG coordinates are influenced by the threshold applied and hence a uniform threshold of $P < 0.001$ (uncorrected) was applied to all fMRI data (lower thresholds were found to yield very large activation cluster for BOLD sessions, whereas higher statistical thresholds could not be passed by ASL-CBF activation clusters). After thresholding, the fMRI activation cluster comprising the peak voxel was identified and the CoG was calculated as *t*-value weighted position.

Group Analysis of fMRI Data

EPI volumes were normalized to the standard template (MNI152 at 2-mm resolution) of the Montreal Neurological Institute (MNI, Canada) using FNIRT (FMRIB's Nonlinear Image Registration Tool). A Gaussian kernel of 4-mm FWHM was used for spatial smoothing. For statistical analysis, we applied FLAME 1 (FMRIB's Local Analysis of Mixed Effects). Z (Gaussianized T/F) statistic images were thresholded using clusters determined by $Z > 2.3$ and a corrected cluster significance threshold of $P < 0.001$. For anatomical assignment, statistics for the contrast "movement vs. baseline" were overlayed with cytoarchitectonic probability maps of the Juelich Histological Atlas [Eickhoff et al., 2007].

Neuronavigated TMS Apparatus

Stereotaxic frameless neuronavigation was performed with the eXimia NBS system Version 2.1.1 (Nexstim, Helsinki, Finland). As subjects performed a thumb abduction task during fMRI, the right abductor pollicis brevis (APB) muscle served as target muscle. Simultaneous electromyographic (EMG) recordings were additionally obtained from the right first dorsal interosseus (FDI) muscle. EMG signals were recorded by Ag/AgCl surface electrodes (Tyco Healthcare, Neustadt, Germany) placed in a belly tendon montage. The EMG signal was amplified, filtered with a 0.5 Hz high-pass filter and digitized using a PowerLab 26 T Myograph and the "Scope" software package Version 3 (ADInstruments, Dunedin, New Zealand). Prior to the study, TMS coils were X-rayed. Displacements between central positions of the outer plastic case and the inner copper wings occurred solely in anterior–posterior (AP) direction and did not exceed 1 mm.

Motor Hotspot and Resting Motor Threshold

Subjects were comfortably seated in an adjustable armchair with head-rest. The head of the subject was coregistered with the individual high-resolution anatomical MR image via anatomical landmarks (e.g., nasion and crus helicis). Prior to the study, the accuracy of the coregistration procedure was verified by small vitamin E capsules (providing a good MRI T_1 contrast) attached to a volunteer's head at different anatomical positions. The software-depicted and true positions of the capsules did not show mismatches larger than 1 mm for any position. Furthermore, the root mean square difference between positions of landmarks in the MRI volume and at the subjects head was reported to be $\leq$2 mm for any TMS session of this study (reported by the neuronavigation software). After anatomical coregistration, the motor "hotspot," i.e., the coil position providing highest MEPs of the APB muscle with shortest latencies during single pulse supra-threshold TMS, was identified. Hotspot coil orientations were (nearly) perpendicular ($90 \pm 10°$) to the central sulcus and tangential to the scalp in all investigated subjects (information provided by the neuronavigation software). The resting motor threshold (RMT) was assessed by means of the TMS Motor Threshold Assessment Tool 2.0 (http://www.clinicalresearcher.org/software.htm) suggested by Awiszus [2003]. The software starts with 45% as stimulator output intensity. After being informed via button press whether a TMS effect (in the present study: a MEP with a peak-to-peak amplitude of at least 50 μV) was induced by

the applied stimulus or not, the software suggests a new threshold intensity based on maximum likelihood calculations. In the present study, the procedure was repeated 12 times ensuring a reliable estimation of the motor threshold (MT).

TMS Motor Mapping

TMS mapping of the dominant, i.e., left motor cortex and the surrounding tissue was obtained by stimulation of an area determined by 8 anterior-posterior (AP) × 7 (medial–lateral) positions spaced at intervals of 10 mm. The hand knob structure [Yousry et al., 1997] was located approximately in the center of the grid, and the AP axis was oriented in parallel to the interhemispheric fissure. Classen et al. [1998] showed that increasing the grid size improves the motor mapping accuracy. Hence, we used a relatively large grid resulting in an area of 7 × 6 cm in size being stimulated. With such a large area stimulated we expected that stimulation of several positions at the margins of the grid would not result in MEPs. Classen et al. [1998] demonstrated that 5–6 stimuli per position are sufficient to achieve stable mapping results. Hence, positions not resulting in a MEP after 5 trials (peak-to-peak amplitude >50 μV) were stimulated with five stimuli, whereas positions resulting in at least one MEP after five trials were stimulated with 10 stimuli to achieve a good trade-off between mapping time and accuracy. The order of stimulation was randomized across the 56 positions [120% RMT; inter stimulus interval (ISI) = 1500 ms]. During the mapping procedure coil tilting was tangentially to the scalp and the TMS coil orientation was identical to coil orientation during RMT identification and stimulation at fMRI maxima coordinates. Both parameters were maintained throughout the mapping procedure.

The mean peak-to-peak MEP amplitude of the APB was calculated for each grid position using all EMG recordings obtained from this position (i.e., either 5 or 10) and divided by the largest amplitude obtained within the stimulation area. Based on these data, the CoG of the APB was calculated using the following formula:

$$\mathrm{CoG} = \left[\sum_i \frac{\bar{a}(x_i, y_i) x_i,}{a_{i,\max}}, \sum_i \frac{\bar{a}(x_i, y_i) y_i,}{a_{i,\max}} \right]$$

with a_i being the mean amplitude at position x_i or y_i [Classen et al., 1998]. While the TMS motor hotspot represents the site of maximal neuronal excitability, the CoG takes into account the spatial distribution of excitability in the pericentral region. Spatial differences between hotspot and CoG locations occur if there is an asymmetrical distribution of excitability around the hotspot. Therefore, the information provided by a CoG is not the location of highest excitability, but the weighted average of excitability of the region of interest. CoG coordinates might be less prone to artifacts, e.g., resulting from co-activation of other muscles. As it is unknown at which position, superficial or deep, TMS-induced neuronal excitation occurs we projected TMS identified positions (i.e., hotspot and CoG positions) onto the cerebral surface. This was done by identifying the individual depth of the cerebral surface by surface peeling of the software generated 3D head model (mean distance from the scalp: 24.5 ± 2.7 mm). Positions with highest electric field (EF) strength at the cerebral surface were recorded during hotspot identification and TMS mapping and used for later analyses. EF_{max} positions were then marked on the individual structural T_1 image and transferred into MNI space by applying the respective nonlinear normalization transform that was also used to transfer individual fMRI activation maps into MNI space.

TMS of Peak Voxel Coordinates at 120% RMT

Brain tissue at fMRI peak voxel coordinates was stimulated with 120% RMT (15 stimuli; ISI = 3000 ms). The order of peak voxels obtained by the three different fMRI sequences was counterbalanced across subjects. The experimenter was blinded to the fMRI sequence. The target entry point for stimulation was identified by bringing the TMS coil in a position in which the distance between fMRI target and EF_{max} value position was found to be minimal (0–2 mm, computed by the software). Then, tilting of the coil was adjusted until the coil was tangential to the scalp (computation and visual feedback provided by the software). TMS coil orientation coincided with TMS coil orientation during RMT identification. In this final position, one stimulus was applied. The coil positioning parameters of this stimulus were used as reference for all subsequent stimuli at this particular target (by means of the "aiming tool" implemented in the neuronavigation software).

RESULTS

fMRI Group Analysis

The fMRI group analysis of the contrast "right thumb movement vs. baseline" revealed a left-lateralized network of cortical areas in left sensorimotor cortex located on the precentral and postcentral gyrus (Fig. 1, $P < 0.001$, cluster-level corrected). SE-BOLD and GRE-BOLD sequences showed additional bilateral activation of the supplementary motor area (SMA), pre-SMA, cingulate motor area, dorsal and superior ventral premotor cortex, and anterior intraparietal cortex. More voxels were activated in the GRE-BOLD cluster as compared to the SE-BOLD cluster, and more for SE-BOLD than for ASL-CBF. The voxel with highest *t*-value at the precentral gyrus assessed in the voxel-wise group analysis of the spatially normalized GRE-BOLD session was close to the crown of the precentral gyrus (Fig. 1, top right) and assigned to Brodman Area 6 (BA6) by the Juelich Histological Atlas (MNI coordinates: −38, −22, 62). In contrast, the peak voxel of the

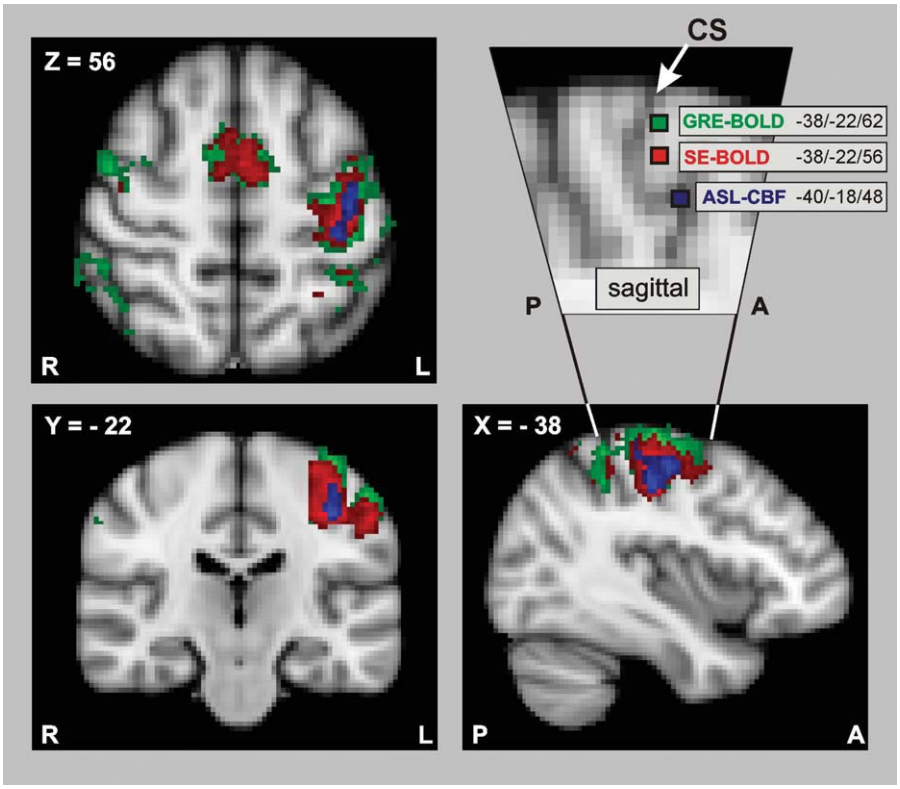

Figure 1.

Results of the fMRI group analysis. Functional magnetic resonance imaging (fMRI) was performed in 15 healthy subjects during right thumb abductions with three different fMRI techniques, i.e., Gradient-Echo (GRE-BOLD, green), Spin-Echo (SE-BOLD, red), and Arterial Spin-Labeling (ASL-CBF, blue). GRE-BOLD and SE-BOLD rely on blood oxygenation level-dependent (=BOLD) contrast, whereas ASL-CBF measures changes in cerebral blood flow (=CBF). "Movement vs. rest" contrasts were superimposed onto the MNI standard template ($P < 0.001$, cluster-level corrected; only voxels exceeding a *t*-threshold of 3.0 are shown). The detail of the sagittal view (top right) shows the voxel with highest statistical *t*-value located within the precentral gyrus for each of the three different fMRI techniques (voxels were projected into plane $X = -38$). In line with our hypotheses, SE-BOLD and ASL-CBF yielded more focused activation with higher specificity than GRE-BOLD. The voxel with highest GRE-BOLD signal change was closest to the gyral surface and was assigned to the premotor cortex (Juelich Histological Atlas). Highest SE-BOLD and ASL-CBF signal changes occurred 6 and 14 mm deeper within the central sulcus, respectively and were assigned to the primary motor cortex (Juelich Histological Atlas). The white arrow marks the central sulcus (CS).

SE-BOLD group analysis was 6 mm deeper within the central sulcus and assigned to area BA4a, i.e., the anterior primary motor cortex (MNI coordinates: −38, −22, 56). The peak voxel of the ASL-CBF group analysis was located even deeper in the central sulcus (14 mm deeper than GRE-BOLD, 8 mm deeper than SE-BOLD group fMRI peak voxels) and assigned to area BA4p, i.e., the posterior part of the primary motor cortex (MNI coordinates: −40, −18, 48).

Individual fMRI Peak Voxel Coordinates

The differences found for the fMRI sequences in the fMRI group analysis were confirmed by analyses based on individual activation maps. Movement-related neural activity could be observed with all three fMRI sequences in all subjects. However, sensitivity in terms of *t*-values of local maxima at the hand knob was significantly different across fMRI sequences [repeated measures ANOVA ($n = 15$)] with the factor "sequence" (levels "GRE-BOLD", "SE-BOLD", and "ASL-CBF"; $F(2, 28) = 64.003$; $P < 0.001$). GRE-BOLD peak voxels had significantly higher *t*-values (11.4 ± 3.8) than SE-BOLD (5.7 ± 2.3) and ASL-CBF (1.6 ± 0.9) peak voxels. SE-BOLD peak voxels had significantly higher *t*-values than ASL-CBF peak voxels (post-hoc paired sample *t*-test, $P < 0.001$, each comparison). However, also the position of the peak voxel coordinates was significantly different across sequences: A repeated

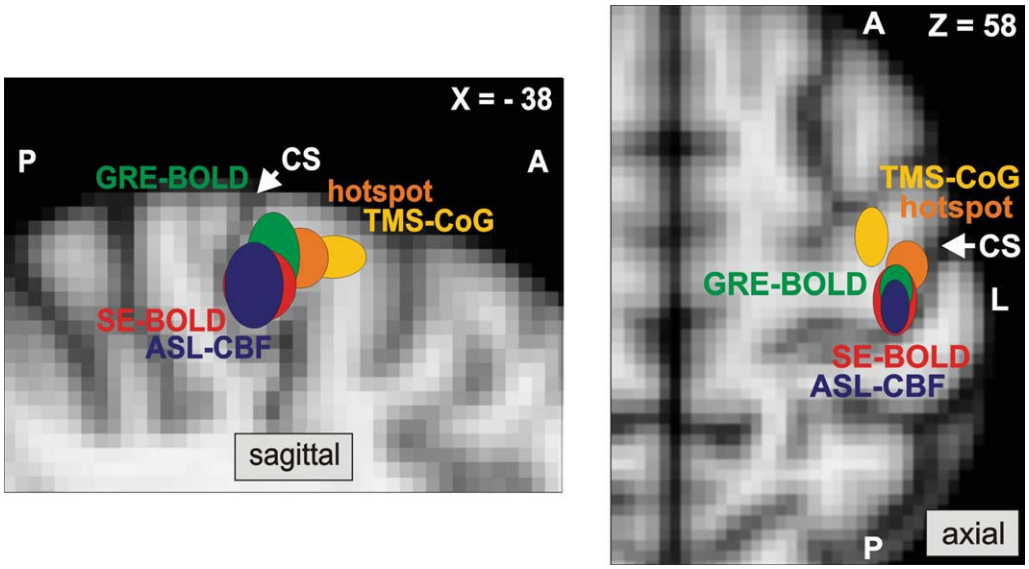

Figure 2.

Localization of the primary motor cortex with fMRI and TMS. Colored ellipsoids indicate mean MNI coordinates (±SD) of fMRI peak voxels and optimal transcranial magnetic stimulation (TMS) positions located within the precentral gyrus of the left hemisphere ($n = 12$ subjects). fMRI peak voxels were defined as voxel with highest statistical *t*-value during right thumb abductions measured with GRE-BOLD (green), SE-BOLD (red), and ASL-CBF (blue). Hotspot coordinates refer to stimulation sites resulting in highest abductor pollicis brevis (APB) muscle responses with shortest latencies (orange). CoG coordinates were calculated from a TMS motor mapping, and reflect the motor-evoked potential weighted maximum electric field coordinate (yellow). All coordinates were projected into sagittal plane $X = -38$ for the figure on the left showing the sagittal view and plane $Z = 58$ for the right figure on the right showing the axial view. GRE-BOLD coordinates were significantly more superficial than SE-BOLD and ASL-CBF coordinates (paired-sample *t*-test, $P < 0.05$, each comparison). Hotspot and CoG coordinates were significantly more anterior than fMRI maxima (paired-sample *t*-test, $P < 0.05$, each comparison). Euclidean distances to hotspot or CoG coordinates were not statistically different for GRE-BOLD, SE-BOLD, and ASL-CBF coordinates (paired-sample *t*-test, $P > 0.05$, each comparison). The white arrow marks the central sulcus (CS).

measures ANOVA ($n = 15$) with the factor "sequence" (levels "GRE-BOLD", "SE-BOLD", and "ASL-CBF") showed significant differences between fMRI peak voxel coordinates in MNI coordinate *Z* [$F(2, 28) = 3.542$, $P < 0.05$; Fig. 2; Table I], i.e., in inferior–superior direction. Post-hoc *t*-tests revealed that GRE-BOLD coordinates (mean MNI coordinate *Z*: 60.7 ± 6.3) were significantly more superficial than SE-BOLD coordinates (56.4 ± 5.0) and ASL-CBF coordinates (55.5 ± 6.6), which were on average 4.3 and 5.2 mm deeper within the central sulcus, respectively ($P < 0.05$, for each comparison). SE-BOLD and ASL-CBF peak voxel coordinates were not statistically different ($P > 0.05$). There were no significant differences between sequences in the other two dimensions, i.e., in the medial–lateral (MNI coordinate *X*; ANOVA, $F(2, 28) = 1.053$; $P > 0.05$) or posterior–anterior direction [MNI coordinate *Y*; ANOVA, $F(2, 28) = 0.829$; $P > 0.05$].

Individual fMRI CoG Coordinates

Significant spatial differences in depth (i.e., in MNI coordinate *Z*) were preserved when similar analyses (repeated measures ANOVA with the factor "sequence") were performed on fMRI CoGs instead of fMRI peak voxels [$F(2, 28) = 4.662$, $P < 0.05$]. Post-hoc *t*-tests revealed that GRE-BOLD CoG coordinates (mean MNI coordinate *Z*: 56.5 ± 2.5) were significantly more superficial than SE-BOLD (50.9 ± 5.5) and ASL-CBF (52.2 ± 6.9) CoG coordinates ($P < 0.05$, each comparison), whereas SE-BOLD and ASL-CBF CoG coordinates were not statistically different (paired sample *t*-test; $P > 0.05$). In addition, there was a significant difference in medial–lateral direction [i.e., in MNI coordinate *X*; $F(2, 28)$

TABLE I. Positions of highest fMRI signals and highest TMS effects individually identified in 12 subjects and transferred into MNI space using nonlinear normalization

	X	Y	Z
GRE-BOLD	−38.4 ± 3.2	−20.6 ± 4.2	60.7 ± 6.3
SE-BOLD	−37.9 ± 3.9	−21.5 ± 5.6	56.4 ± 5.0
ASL-CBF	−37.6 ± 2.6	−22.9 ± 4.5	55.5 ± 6.6
TMS hotspot	−40.7 ± 4.3	−15.7 ± 3.8	59.7 ± 3.7
TMS CoG_{APB}	−33.4 ± 2.7	−10.9 ± 5.0	60.0 ± 2.6

TABLE II. Euclidean distances between fMRI and TMS sites in single subject space

	fMRI peak voxel vs. TMS hotspot			fMRI CoG vs. TMS CoG		
Subjects	GRE	SE	ASL	GRE	SE	ASL
1	11.49	15.10	13.75	42.89	17.80	21.29
2	12.81	4.90	13.56	8.50	14.73	21.00
3	14.59	14.59	13.00	14.18	14.56	15.98
4	13.75	13.75	9.43	14.49	18.60	8.95
5	7.48	7.48	17.80	17.68	24.49	19.78
6	11.00	6.32	11.49	23.86	12.66	3.84
7	8.72	14.70	13.75	25.54	12.22	11.17
8	5.48	17.15	18.47	22.22	25.30	24.58
9	13.19	13.19	16.67	19.25	25.87	23.75
10	11.45	10.77	10.05	5.20	5.85	17.56
11	6.40	6.32	8.94	5.75	11.77	8.89
12	9.38	10.20	6.32	17.93	22.11	20.53
Mean	10.5	11.2	12.8	18.1	17.2	16.4
SD	3.0	4.1	3.7	10.3	6.3	6.7

$= 5.948$, $P < 0.05$] as GRE-BOLD CoGs were significantly more medial than SE-BOLD and ASL-CBF CoG coordinates (paired sample *t*-tests; $P < 0.05$, each comparison). SE-BOLD and ASL-CBF CoG coordinates were not statistically different in medial–lateral direction (paired sample test; $P > 0.05$). There were no statistically significant differences between sequences in AP localization (i.e., MNI coordinate *Y*) of CoGs [$F(2, 28) = 0.572$; $P > 0.05$].

Differences in fMRI and TMS Positions

For each subject, the TMS coordinate of the motor "hotspot" i.e., the coil position and tilt for evoking a MEP of 50 μV peak-to-peak amplitude with lowest stimulator output intensity) and the CoG of a systematic TMS mapping of the motor cortex were projected into MNI space applying the individual FNIRT registration transform. MNI coordinates were then compared with the fMRI peak voxel coordinates by computing a repeated measures ANOVA ($n = 12$) with the factor "localization approach" (levels "CoG_{APB}," "hotspot," "GRE-BOLD," "SE-BOLD," and "ASL-CBF"). The analyses revealed significant differences in medial–lateral direction, i.e., in MNI coordinate *X* [$F(4, 44) = 8.705$; $P < 0.001$) and in AP direction, i.e., in MNI coordinate *Y* [$F(4, 44) = 14.168$; $P < 0.001$]. Differences in inferior-superior direction, i.e., MNI coordinate *Z* showed a statistical trend [$F(4, 44) = 2.353$; $P = 0.069$; Table I]. Bonferroni-corrected post-hoc *t*-tests revealed that the motor hotspot was significantly anterior to GRE-BOLD, SE-BOLD, and ASL-CBF coordinates ($P < 0.05$, each comparison; Fig. 2). Displacements between fMRI maxima and the hotspot in medial-lateral direction were less pronounced but there was a statistical trend for hotspot coordinates to be more lateral than fMRI maxima ($P < 0.100$, each comparison). Hotspot coordinates were assigned to BA6 in all 12 subjects (Juelich Histological Atlas). The CoG_{APB} was significantly anterior to hotspot, GRE-BOLD, SE-BOLD, and ASL-CBF coordinates ($P < 0.05$, each comparison). In addition, CoG_{APB} coordinates were significantly more medial than ASL-CBF, GRE-BOLD, and hotspot coordinates ($P < 0.05$, each comparison) whereas the comparison to SE-BOLD coordinates failed the corrected *P*-threshold of $P < 0.007$ only marginally ($P = 0.011$, uncorrected). In all 12 subjects the CoG_{APB} was assigned to BA6.

Euclidean Distances Between fMRI and TMS Positions

Although we found spatial differences between fMRI maxima obtained by different fMRI sequences, Euclidean distances between these maxima and the TMS hotspot were not statistically different across sequences [GRE-BOLD: 10.5 ± 3.0 mm; SE-BOLD: 11.2 ± 4.1 mm; ASL-CBF: 12.8 ± 3.7 mm; $F(2, 22) = 1.360$; $P > 0.05$, repeated measures ANOVA; see also Table II]. The same was true for Euclidean distances between fMRI maxima and the TMS mapping CoG_{APB},, which were also not significantly different across sequences [GRE-BOLD: 13.4 ± 5.5 mm; SE-BOLD: 15.3 ± 5.7 mm; ASL-CBF 15.3 ± 7.0 mm; $F(2, 22) = 1.115$; $P > 0.05$, repeated measures ANOVA]. In other words, none of the fMRI sequences localized neural activity systematically closer to the TMS hotspot or the TMS CoG_{APB}.

If identical analyses were conducted with fMRI CoGs instead of fMRI peak voxels, results were similar, i.e., none of the fMRI sequences yielded CoG positions systematically closer to the TMS hotspot [$F(2, 22) = 1.151$; $P > 0.05$] or CoG_{APB} [$F(2, 22) = 0.191$; $P > 0.05$; see also Table II].

TMS of fMRI Peak Voxel with 120% RMT

We stimulated brain tissue at the fMRI peak voxel coordinate with single-pulse neuronavigated TMS to investigate whether the spatial differences found for the three different fMRI sequences are functionally relevant, i.e., impact on MEP size of the respective peripheral muscle. A repeated measures ANOVA ($n = 12$) with the factors "sequence" and "muscle" (levels "APB" and "FDI") yielded a significant main effect of sequence [$F(22, 2) = 4.797$; $P < 0.05$] and muscle [$F(11, 1) = 8.506$; $P < 0.05$] but no significant interaction [$F(22, 2) = 0.131$; $P > 0.05$]. Post-hoc *t*-tests revealed that mean peak-to-peak MEP amplitudes of the APB and the FDI were higher for GRE-BOLD coordinates compared to both SE-BOLD coordinates and ASL-CBF coordinates ($P < 0.05$, each comparison; Fig. 3A). Muscle responses during TMS of SE-BOLD and ASL-CBF coordinates were not statistically different ($P > 0.05$). MEPs of the APB were statistically higher than MEPs of

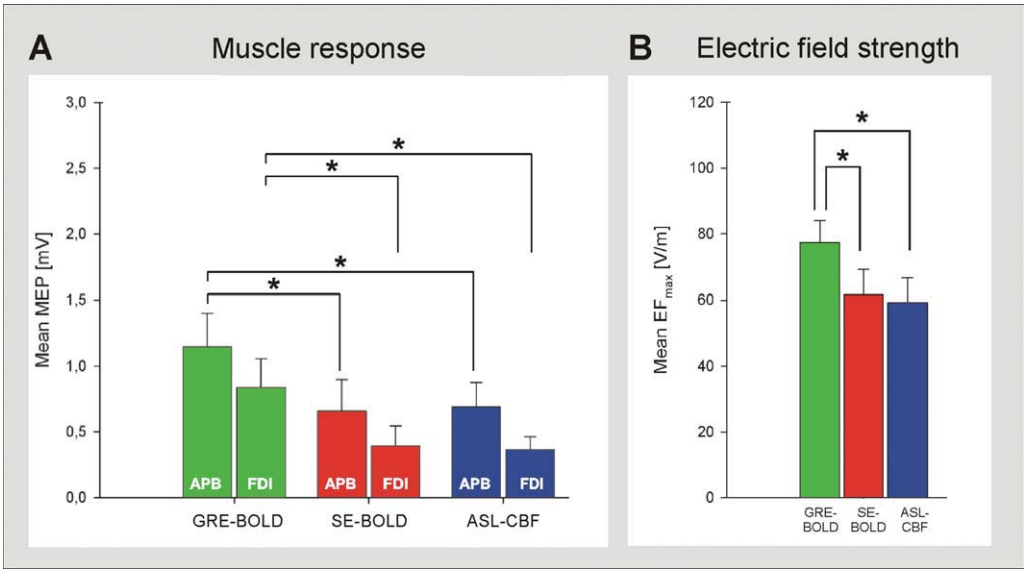

Figure 3.

Stimulation of brain tissue at fMRI peak voxel coordinates with TMS. Neuronavigated TMS (120% resting motor threshold) was used to stimulate brain tissue at fMRI peak voxel coordinates to investigate whether localization differences between fMRI sequences are functionally relevant, i.e., impact on muscle responses ($n = 12$ subjects). **A**: Muscle responses. Peak-to-peak motor-evoked potentials (MEPs) of the abductor pollicis brevis (APB) and the first dorsal interosseus (FDI) hand muscle are shown. MEPs resulting of stimulation at GRE-BOLD coordinates were significantly higher than MEPs resulting of stimulation at SE-BOLD and ASL-CBF coordinates. **B**: Electric field strength at target position. Maximum electric field values (EF_{max}) reaching the fMRI target position during stimulation are shown. GRE-BOLD coordinates were stimulated with significantly higher EF_{max} values than SE-BOLD and ASL-CBF coordinates which were significantly deeper in the central sulcus and hence further away from the TMS coil. Mean EF_{max} values during stimulation at SE-BOLD and ASL-CBF coordinates were not statistically different (paired-sample *t*-test, $P > 0.05$). Error bars indicate standard errors. Asterisks indicate significant differences in paired sample *t*-tests (paired-sample *t*-test, $P < 0.05$, each comparison).

the FDI during stimulation of SE-BOLD and ASL-CBF coordinates ($P < 0.05$, each comparison) but not during stimulation of GRE-BOLD coordinates ($P > 0.05$). In summary, spatial differences of local maxima were matched by functional differences in MEP amplitudes. TMS at GRE-BOLD coordinates was probably more effective than TMS at SE-BOLD or ASL-CBF coordinates because GRE-BOLD coordinates were more superficial and anterior, and hence closer to optimal TMS positions than SE-BOLD and ASL-CBF sites. We correlated individual differences in mean MEPs obtained by stimulation of GRE-BOLD vs. SE-BOLD positions with individual spatial differences of GRE-BOLD vs. SE-BOLD positions in AP direction. The result suggests that TMS over the GRE-BOLD site evoked larger MEPs the more anterior the GRE-BOLD coordinate was (APB: Pearson's $r = 0.67$, $P < 0.05$; FDI: Pearson's $r = 0.63$, $P < 0.05$). However, correlations for differences of GRE-BOLD vs. ASL-CBF positions and SE-BOLD vs. ASL-CBF positions were not statistically significant ($P > 0.05$, each correlation). Differences in medial–lateral or inferior–superior direction were not significantly correlated with differences in MEP amplitudes between the three different fMRI sites ($P > 0.05$, each correlation). However, a significant main effect of sequence in the repeated measures ANOVA on mean EF_{max} values at the target position during TMS ($F(22, 2) = 5.779$; $P < 0.05$) indicates that due to the physical constraints of TMS, superficial GRE-BOLD coordinates were stimulated with significantly higher mean EF_{max} values (77.4 ± 23.2 V/m) compared to deeper SE-BOLD (61.7 ± 26.5 V/m) and ASL-CBF coordinates (59.2 ± 25.9 V/m; paired sample *t*-tests, $P < 0.05$, each comparison; Fig. 3B). Differences between SE-BOLD and ASL-CBF coordinates in EF_{max} values were not statistically significant (paired sample *t*-test, $P > 0.05$).

Tests to Exclude Spatial Errors of the TMS Equipment

Coregistration quality was verified prior to the study and after each session (to verify that the head tracker depicting the subject's head position had not changed its position during the TMS session). Furthermore, for one subject with pronounced anterior shift of the optimal TMS position (Subject 1, see Fig. 4), the complete motor mapping was repeated with the induced current direction as

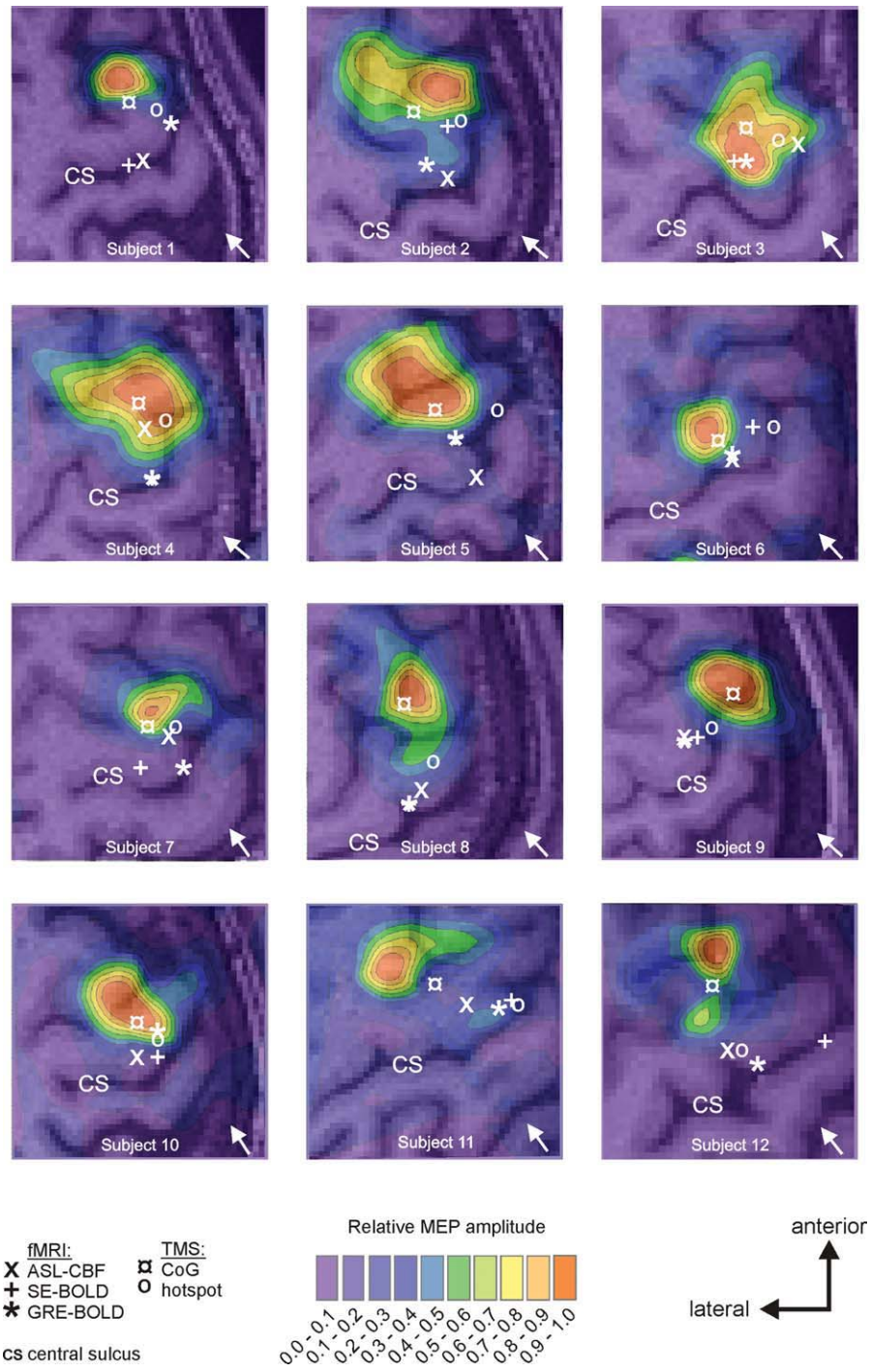

Figure 4.

Results of TMS motor mappings. Eight (anterior–posterior) × seven (medial–lateral) positions spaced at intervals of 10 cm were stimulated with neuronavigated TMS in randomized order (10 stimuli if at least one MEP $>$ 50 μV was recorded after five stimuli; otherwise five stimuli; 120% RMT; ISI $=$ 1500 ms). The hand knob was located approximately in the center of the grid, and the anterior–posterior axis was oriented in parallel to the interhemispheric fissure. Positions refer to electric field maximum (EF_{max}) positions within the cerebral cortex calculated by computerized modeling. Contours represent 10 percentiles of the averaged maximal response of the APB muscle viewed from above. Background images refer to individual structural images showing the corresponding underlying cerebral anatomy. All fMRI and TMS positions (depicted as white symbols) were projected into the slice corresponding to the mean axial depth of all five individual sites (i.e., GRE-BOLD, SE-BOLD, ASL-CBF, hotspot, and CoG).

applied before (i.e., PA, perpendicular to the central sulcus) and additionally with inverted induced current direction (i.e., AP, perpendicular to the central sulcus). If systematic anterior EF distortions due to coil failure or inaccurate computerized modeling accounted for the anterior shift of the optimal TMS position, then the CoG of the mapping with inverted coil orientation (AP-induced current direction) should be located considerably more posterior (i.e., to the amount of the displacement) than with standard coil orientation. The results showed that except for a drop in maximum MEP size, we basically replicated the map recorded with PA-induced current direction with almost identical location of peak excitability and CoG (Supporting Information Fig. 1). Therefore, technical confounds cannot explain the systematic anterior shift of optimal TMS positions when compared to fMRI peak voxels.

DISCUSSION

Localization Differences Between fMRI Sequences

Localization of the motor hand area

The primary motor cortex is a cortical key area for the execution of voluntary movements [Dum and Strick, 2002; Grefkes et al., 2008; Sanes and Donoghue, 2000]. This region is structurally well defined: Human post-mortem studies showed that the primary motor cortex (BA4) is a distinct cytoarchitectonic area characterized by the absence of layer IV and presence of giant Betz cells in layer V [Brodmann, 1909]. At the hand representation area, BA4 is buried within the central sulcus and rarely extends to the gyral surface [Geyer et al., 1996] where it forms a sharp boundary with the premotor cortex. As ASL-CBF and SE-BOLD showed highest signal increase during isolated simple thumb abductions in the rostral wall of the central sulcus, i.e., the location where BA4 has to be expected [Eickhoff et al., 2007], our data suggest that at 3 T these fMRI sequences may correctly locate the primary motor hand area. By contrast, signal increases for the GRE-BOLD sequence were shifted towards the crown of the precentral gyrus, and thus, towards premotor areas.

Systematic Superior Shift of GRE-BOLD

Both, fMRI group analysis as well as single subject fMRI analyses, demonstrated that highest GRE-BOLD signal changes showed a systematic shift in superior direction. These findings suggest that the underlying cause is, at least partially, subject-independent. High susceptibility of GRE-BOLD for large draining veins [Boxerman et al., 1995; Uludag et al., 2009] mainly running on the cerebral surface [Duong et al., 2000] seem to be the most likely explanation for our findings.

Spatial Localization of ASL-CBF (vs. GRE-BOLD) Signal

ASL sequences measure CBF by means of magnetically labeled arterial water that has either passed the capillary wall into tissue or is still located within capillaries [Silva et al., 1997]. Due to the tight neurovascular coupling, ASL-CBF changes have been shown to occur in close proximity to neuronal activity [Duong et al., 2000; Luh et al., 2000; Tjandra et al., 2005]. The main disadvantage of ASL-CBF over GRE-BOLD is decreased sensitivity. We used a robust block design and relatively long scanning durations of 11 min with only one condition to accomplish this problem, but being able to use equal experimental conditions (i.e., scanning times) for all fMRI sequences. Pilot experiments on healthy volunteers showed that shorter scanning times resulted in lower sensitivity whereas longer scanning times rather increased fatigue of the subjects and head movement artifacts with only minor gain in sensitivity (as the signal-to-noise ratio increases in proportion to the square root of the number of acquisitions, i.e., doubling SNR means four times longer scanning times). We, therefore, used a scanning duration of 11 min as trade off between evoking sufficient fMRI signal and duration of the whole fMRI experiments (which was 40 min on average (including structural images and localizers). However, the low sensitivity of ASL-CBF measurements did apparently not affect spatial localization accuracy which was found to be clearly superior over GRE-BOLD. Duong et al. [2000] compared GRE-BOLD and ASL-CBF signal changes during forepaw stimulation in anesthetized rats at 9.4 T and in line with our findings, GRE-BOLD signal was more expanded and located at the cortical surface whereas voxels with highest ASL-CBF percent signal changes showed excellent spatial co-localization with synaptic activity within deeper cortical layers [measured by means of manganese ion (Mn^{2+}) acting as calcium analogue and MRI contrast agent]. Interestingly, Luh et al. [2000] identified tissue types by means of T_1 maps and demonstrated that T_1-values were correlated on a voxel-wise basis with BOLD and ASL-CBF signal changes in healthy subjects at 3 T. For GRE-BOLD especially voxels with highest *t*-values predominantly contained cerebrospinal fluid (CSF) and/or blood. In contrast, highest relative ASL-CBF signal changes were located in voxels with T_1-values similar to voxels containing predominantly grey matter. In addition, Luh et al. [2000] demonstrated that BOLD and ASL-CBF activation maps showed a fractional overlap of only 40%. In contrast, Tjandra et al. [2005] found no statistical spatial displacement between GRE-BOLD and ASL-CBF statistical *t*-maps in healthy subjects at 3 T. However, Tjandra et al. [2005] used center-of-gravities (CoGs) instead of peak voxel coordinates. The findings of Luh et al. [2000] that especially voxels with high statistical values may contain signal from large veins and CSF, suggest that a venous

shift might have been evident when comparing peak voxels instead of CoGs. We, however, found no support for this suggestion in the present study as the results of analyses with fMRI peak voxels were preserved in analyses with fMRI CoGs, i.e., fMRI coordinates showed differences in depth but not in Euclidean distances to optimal TMS positions. Nevertheless, Tjandra et al. [2005] also defined the nearest draining vein by MR venograms and found that GRE-BOLD signal was significantly closer to draining veins than ASL-CBF signal. Thus, our data are supported by growing body of evidence that ASL-CBF is better co-localized to neural activity, whereas GRE-BOLD is susceptible to shifts towards large veins or CSF.

Localization of SE-BOLD vs. GRE-BOLD

SE-BOLD and GRE-BOLD fMRI sequences are both sensitive to the BOLD effect—a joint combination of changes in blood volume, CBF, and de-oxygenation level of blood [Buxton et al., 1998]. At 1.5 and 3 T, both sequences have high susceptibility for large draining veins [Kennan et al., 1994; Boxerman et al., 1995; Oja et al., 1999; Uludag et al., 2009]. From 3 T upwards, intravascular signal from veins vanishes for SE-BOLD, but not GRE-BOLD [Uludag et al., 2009]. Intra- and extravascular contributions to SE-BOLD signal changes are equal at 3 T [Norris et al., 2002] but intravascular signals mainly arise from microvasculature (i.e., capillaries, arterioles, and venules). Although intravascular signal also decreases with increasing field strength for GRE-BOLD, there is no field strength at which the BOLD signal from the microvasculature is larger than from the macrovasculature [Uludag et al., 2009]. Recent high magnetic field studies in rats [Lee et al., 2002] and humans [Duong et al., 2002] demonstrated that both SE-BOLD and ASL-CBF located neural activity within grey matter with good spatial correspondence suggesting that SE-BOLD provides comparable high spatial specificity as ASL-CBF. Several studies investigating the laminar specificity of high-resolution SE-BOLD and GRE-BOLD fMRI in primary visual cortex of macaque monkeys [Goense and Logothetis, 2006] and cats [Harel et al., 2006] at 4.7 and 9.4 T, respectively demonstrated laminar specific activation for SE-BOLD yielding highest signal changes in cortical layer IV whereas highest GRE-BOLD signal changes occurred at the cerebral surface. However, studies comparing different fMRI sequences in humans at 3 T are scarce [Thulborn et al., 1997]. Thulborn et al. [1997] measured neural activity during stimulation with different visual stimuli and found that the 10 most significant voxels obtained with SE-BOLD and GRE-BOLD overlapped by only 30–40%. This result suggests that SE-BOLD signal is not just a subset of the more sensitive GRE-BOLD activation, but that both detect spatially different effects. This finding is in good agreement with our data suggesting that already from 3 T on, SE-BOLD signal changes are well localized with primary motor cortex activity. Uludag et al. [2009] showed that reduced macro-vasculature weighting is achieved if large vessels predominantly run parallel to the main magnetic field as the susceptibility effect equals to zero for this condition. This is, for example, true for the central sulcus and hence for parts of the motor cortex but not, e.g., for the calcarine sulcus where the large vessels are mainly oriented perpendicular to the magnetic field. Therefore, in our study, SE might be more sensitive to gray matter than large vessels.

Taken together our findings strongly encourage considering alternative fMRI sequences such as ASL-CBF and (under certain conditions) SE-BOLD when spatial localization is of high priority. However, decisions may depend on multiple aspects and not only on localization (Table III). For example, ASL-CBF is superior to GRE-BOLD in spatial accuracy, provides lower inter-session and inter-subject variation [Tjandra et al., 2005], and offers quantitative measures, in contrast to GRE-BOLD [Kim et al., 1997; Luh et al., 1999]. However, GRE-BOLD offers highest sensitivity (in terms of contrast-to-noise ratio), temporal resolution (due to faster data acquisition) and finally, a larger number of slices can readily measured with GRE-BOLD, whereas ASL-CBF is limited to fewer slices [Liu and Brown, 2007].

Localization Differences Between fMRI and TMS

Surprisingly, although SE-BOLD and ASL-CBF were more accurate in anatomical localization of the primary motor hand area, they provided significantly lower muscle responses than GRE-BOLD when stimulated with TMS. One explanation may be found in the properties of the EF induced by the magnetic pulse which declines exponentially with increasing distance from the coil [Eaton, 1992]. As GRE-BOLD peak voxel coordinates were significantly more superior (i.e., closer to the TMS coil), they were stimulated with significantly higher EF strengths than SE-BOLD and ASL-CBF peak voxels. In this case, stimulation under equal conditions seems impossible to achieve with TMS, as stimulation of maxima with similar EF values would require stimulation with highly differently stimulator output intensities, thereby enlarging the stimulated area. However, as it is unknown at which position, superficial or deep, excitation occurs accounting for highest TMS effects [Fox et al., 2004; Salinas et al., 2009; Thielscher and Wichmann, 2009], the most likely explanation for our findings is that the GRE-BOLD site was located more anterior (i.e., closer to the TMS hotspot) and thus TMS at the GRE-BOLD site was more effective. However, spatial distances between fMRI peak voxels and optimal TMS positions, i.e., hotspots and mapping CoGs, were not statistically different across fMRI sequences. This finding demonstrates that the mismatch between TMS and fMRI persists even if fMRI sequences with high anatomical accuracy such as ASL-CBF or SE-BOLD are used. Hence, a

TABLE III. Qualitative comparison of different motor mapping approaches

	fMRI			TMS
Aim	Identification of position with highest task-related neural activity			Identification of position with lowest electrophysiological threshold to elicit MEPs of the respective peripheral muscle
Assessed via	Neurovascular coupling		ASL-CBF	Cortico-spinal excitability
	GRE-BOLD	SE-BOLD		
Measured variable(s)	BOLD (Deoxy-Hb, CBF, CBV)	BOLD (Deoxy-Hb, CBF, CBV)	CBF	Peripheral EMG signals
Main advantages	High CNR	High spatial specificity	High spatial specificity	Independent of vascular effects
Main disadvantages	Low spatial specificity	Low CNR	Low CNR	Restricted to superficial areas (limited penetration depth)
Main source of signal	Large draining veins	Microvasculature (≥3 T)	Arterioles and capillaries	Indirect trans-synaptic excitation of cell bodies and direct excitation of axons
Localized structure	BA6	BA4a	BA4p	BA6
Distance to surface	+	++	+++	n/a

Please see text body for references.

potential shift of GRE-BOLD towards superficial veins cannot explain the spatial mismatch observed between TMS and fMRI. Although fMRI and TMS were not expected to yield exactly identical positions due to apparent technical differences underlying these two brain mapping approaches, spatial mismatches were considerably large, i.e, 11.9 mm and optimal TMS positions were located within premotor areas in all 12 subjects [Eickhoff et al., 2007]. These differences are not likely to be caused by technical issues, such as systematic coregistration errors or systematic EF distortions in the posterior direction, since the magnitude of displacements were highly different across subjects (e.g., low in Subject 6, and high in Subject 8; Fig. 4). Furthermore, similar anterior displacements were also reported in previous studies investigating spatial congruency of TMS and neuroimaging data such as PET [Classen et al., 1998] and fMRI [Herwig et al., 2002; Lotze et al., 2003]. Even if no precise specifications were made, figures in papers often suggested anterior displacements of optimal TMS positions relative to PET (Wassermann et al. [1996]; Fig. 2) or fMRI (Bastings et al. [1998]; Figs. 2 and 3) activations.

Possible Explanations for the Anterior Shift of Optimal TMS Positions

Muscle responses evoked by TMS typically have up to 3 ms longer latencies than muscle responses evoked by electrical stimulation, which led to the assumption that TMS activates cortical cells predominantly trans-synaptically, whereas electrical stimuli excite cortical cell bodies or axons directly [Day et al., 1989; Hess et al., 1987; Mills et al., 1992; Rothwell et al., 1991]. However, it is unknown whether the entire synaptic chain (from optimal stimulation position to descending motoneurons) is located within the primary motor cortex or whether it includes (inter-) neurons in other regions, e.g., premotor cortex projecting onto BA4 neurons. Hence, although it seems unlikely, it cannot be ruled out that indirect stimulation of BA4 neurons via trans-synaptic input from BA6 accounts for anterior positions of optimal TMS sites.

Although fMRI and TMS sessions were performed under different functional motor states, ("active" during fMRI sessions, "passive" during TMS sessions) this difference seems unlikely to account for the spatial mismatch observed since previous studies demonstrated that TMS mappings under low-level voluntary contraction (10–20% of maximum contraction) yield CoGs significantly anterior (and non-significantly medial) of CoGs obtained at rest [Lewko et al., 1996; Wilson et al., 1995). This anterior–medial shift (in the range of 6.6–20 mm) could be caused by decreased thresholds for surrounding premotor and SMAs during muscle pre-activation [Lewko et al., 1996]. However, this anterior–medial shift would have more likely enlarged than shortened the distance between fMRI and TMS positions in the present study, as TMS mapping

CoGs showed already (predominantly) anterior displacements.

We rather assume that EF effects are likely to account for the anterior shift of optimal TMS positions. Like the neuronavigation system used in the present study, most systems compute EF strength based on spherical head models which assume that EF is maximal directly under the junction of the wings and declines exponentially with distance from the coil [Eaton, 1992]. However, there is growing evidence that this simplified model is insufficient, as different tissue types of the head have different conductivities which change the EF considerably. Realistic head models such as tissue-segmented MR images with realistic anatomical features like gyri and sulci demonstrated that the EF forms a complex pattern onto the folded cerebral cortex [Salinas et al., 2009]. For instance, secondary EFs with either decreasing or increasing effects of varying magnitude (20–35% of primary EF) and direction (often opposing the primary EF) occur especially near tissue boundaries [Salinas et al., 2009]. These data show that stimulation with highest EF intensities does not necessarily occur directly under the junction of the coil as proposed by spherical head models. Therefore, it might be that stimulation with highest EF strength did not necessarily occur directly at the CoG position.

The neurophysiology of TMS is still incompletely understood but there is some evidence that medial-lateral induced current directions activate cortical motor neurons directly leading to D-waves whereas PA-induced current directions, as used in the present study, activate cortical motor neurons predominantly indirectly via interneurons leading to I-waves [Di Lazzaro et al., 1998]. However, at stimulus intensities above the MT, as applied in the present study, induced PA current direction can also excite neurons directly generating D-waves [Di Lazzaro et al., 1998]. Hence, for the coil orientation and stimulus intensity used in the present study both types of neuronal excitation (direct and indirect) should be considered. I-wave generation relies on short distance (inter)neuron or even microscopic (dendrite, cell body) geometry [Herbsman et al., 2009], and there is some evidence that especially these short distance neuronal structures are subject to orientation-specific effects [Amassian et al., 1998]. For instance, Fox et al. [2004] demonstrated that the orientation of the EF relative to cortical columns outweighs highest absolute EF strengths, i.e., TMS excitation was optimal within sulci where cortical columns run parallel to EF direction, although the absolute EF was higher at gyral crowns (where orientation to cortical columns is less optimal). Direct excitation on the other hand is mediated by longer neuronal structures, i.e., axons. Here, inhomogenities of the applied electric field caused by changes of the axonal trajectory relative to the EF are the most dominant factor in TMS-induced neuronal excitability [Amassian et al., 1992; Abdeen and Stuchly, 1994; Maccabee et al., 1993]. Axons originating from BA4 first run perpendicular and anterior to the sulcal wall, and then turn approximately 90° downwards to form the cord fibres and the subcortical bundle in the center of the precentral gyrus [Schmahmann and Pandya, 2006]. Therefore, if for some subjects axonal thresholds were lower due to more abrupt white matter bendings [Fox et al., 2004], these subjects would show an anterior shift of optimal TMS excitation spots. In line with this suggestion are also the results of a very recent study by Herbsman et al. [2009] who investigated the relation between TMS excitability (i.e., MT) and several anatomical parameters in 17 subjects. Approximately 50–60% of the inter-subject variability in MT can be explained by the subjects' individual skull-to-cortex distance [Kozel et al., 2000] but there is also strong evidence that the anterior component of the corticospinal tract is an additional important predictor for MT accounting for ~48% of the variance observed [Herbsman et al., 2009]. Pronounced anterior components of the corticospinal tract were associated with low MT [Herbsman et al., 2009] suggesting that TMS with PA induced current direction may act directly on axons running anterior of BA4 and changing their trajectory relative to the EF.

Implications and Limitations

In summary, we conclude from the findings of the current study that the spatial mismatch between fMRI and TMS is not caused by the venous shift of GRE-BOLD signal. Spatial differences between fMRI and TMS are likely to result from different underlying physiological processes, i.e., fMRI predominantly reflects the position with highest task-related synaptic activity [Duong et al., 2000] at cell bodies, i.e, within grey matter, whereas TMS mappings yield optimal positions for neuronal excitation with applied EFs. These two positions might be different for several reasons including (i) EF distortion (caused by tissue boundaries, etc.) and (ii) direct excitation of axons [Di Lazzaro et al., 1998] which might be distant from cell bodies in white matter. However, if fMRI-based coordinates are more appropriate TMS intervention sites than TMS hotspots remains to be tested in future. One limitation of the present study might be the fact that effects are EF orientation (and hence coil orientation) specific. Our finding that optimal TMS positions were more anterior might not apply to TMS mappings with other coil orientations. EFs in the coronal plane are more likely to act on medial-lateral fiber tract components, and hence might show displacements in medial-lateral direction in contrast to EFs in PA (or AP) directions which predominantly act on AP fiber tract components [Herbsman et al., 2009]. Another limitation of the present study might be that fMRI and TMS sessions were not matched in functional state although fMRI informed TMS lesion studies usually use the same task for the MRI localizer and the TMS experiment. Although this limitation is unlikely to account for the mismatch between fMRI and TMS sites observed in

the present study, it might limit the significance of our findings with respect to previous fMRI-informed (r)TMS studies. Nevertheless, our findings also have implications for studies in which optimal TMS positions cannot be identified as easily as for the motor or visual cortex. Although fMRI-informed TMS might not reflect the optimal position to generate TMS effects, our data indicate that it provides a position resulting in measurable TMS effects, and hence fMRI informed TMS should be preferred to the sole use of structural landmarks. Furthermore, our data imply that if behavioral effects are absent after rTMS over fMRI-based coordinates (e.g., in a cognitive task), missing effects might also result from suboptimal stimulation of the target region due to the spatial mismatch of fMRI coordinates and maximal TMS effects as demonstrated for the motor system in the present study.

ACKNOWLEDGMENTS

The authors thank Kurt Wittenberg and Eva-Maria Hohl for technical support and assistance during the fMRI and TMS sessions.

REFERENCES

Abdeen MA, Stuchly MA (1994): Modeling of magnetic field stimulation of bent neurons. IEEE Trans Biomed Eng 41:1092–1095.

Amassian VE, Eberle L, Maccabee PJ, Cracco RQ (1992): Modelling magnetic coil excitation of human cerebral cortex with a peripheral nerve immersed in a brain-shaped volume conductor: The significance of fiber bending in excitation. Electroencephalogr Clin Neurophysiol 85:291–301.

Amassian VE, Cracco RQ, Maccabee PJ, Cracco JB, Rudell AP, Eberle L (1998): Transcranial magnetic stimulation in study of the visual pathway. J Clin Neurophysiol 15:288–304.

Awiszus F (2003): TMS and threshold hunting. Suppl Clin Neurophysiol 56:13–23.

Barker AT, Jalinous R, Freeston IL (1985): Non-invasive magnetic stimulation of human motor cortex. Lancet 1:1106–1107.

Bastings EP, Gage HD, Greenberg JP, Hammond G, Hernandez L, Santago P, Hamilton CA, Moody DM, Singh KD, Ricci PE, Pons TP, Good DC (1998): Co-registration of cortical magnetic stimulation and functional magnetic resonance imaging. Neuroreport 9:1941–1946.

Boxerman JL, Bandettini PA, Kwong KK, Baker JR, Davis TL, Rosen BR, Weisskoff RM (1995): The intravascular contribution to fMRI signal change: Monte Carlo modeling and diffusion-weighted studies in vivo. Magn Reson Med 34:4–10.

Buxton RB, Wong EC, Frank LR (1998): Dynamics of blood flow and oxygenation changes during brain activation: the balloon model. Magn Reson Med 39:855–864.

Boroojerdi B, Foltys H, Krings T, Spetzger U, Thron A, Topper R (1999): Localization of the motor hand area using transcranial magnetic stimulation and functional magnetic resonance imaging. Clin Neurophysiol 110:699–704.

Brodmann K (1909): Vergleichende Lokalisationslehre der Grosshirnrinde: In Ihren Principien dargestellt auf Grund des Zellenbaues. Leipzig: Johann Ambrosius Barth Verlag.

Cavusoglu M, Pfeuffer J, Ugurbil K, Uludag K (2009): Comparison of pulsed arterial spin labeling encoding schemes and absolute perfusion quantification. Magn Reson Imaging 27: 1039–1045.

Classen J, Knorr U, Werhahn KJ, Schlaug G, Kunesch E, Cohen LG, Seitz RJ, Benecke R (1998): Multimodal output mapping of human central motor representation on different spatial scales. J Physiol 512 (Pt 1):163–179.

Day BL, Dressler D, Maertens de Noordhout A, Marsden CD, Nakashima K, Rothwell JC, Thompson PD (1989): Electric and magnetic stimulation of human motor cortex: surface EMG and single motor unit responses. J Physiol 412:449–473.

Di Lazzaro V, Oliviero A, Profice P, Saturno E, Pilato F, Insola A, Mazzone, Tonali P, Rothwell JC (1998): Comparison of descending volleys evoked by transcranial magnetic and electric stimulation in conscious humans. Electroencephalogr Clin Neurophysiol 109:397–401.

Dum RP, Strick PL (2002): Motor areas in the frontal lobe of the primate. Physiol Behav 77:677–682.

Duong TQ, Silva AC, Lee SP, Kim SG (2000): Functional MRI of calcium-dependent synaptic activity: Cross correlation with CBF and BOLD measurements. Magn Reson Med 43:383–392.

Duong TQ, Yacoub E, Adriany G, Hu X, Ugurbil K, Vaughan JT, Merkle H, Kim SG (2002): High-resolution, spin-echo BOLD, and CBF fMRI at 4 and 7 T. Magn Reson Med 48:589–593.

Eaton H (1992): Electric field induced in a spherical volume conductor from arbitrary coils: Application to magnetic stimulation and MEG. Med Biol Eng Comput 30:433–440.

Eickhoff SB, Paus T, Caspers S, Grosbras MH, Evans AC, Zilles K, Amunts K (2007): Assignment of functional activations to probabilistic cytoarchitectonic areas revisited. Neuroimage 36: 511–521.

Forman SD, Cohen JD, Fitzgerald M, Eddy WF, Mintun MA, Noll DC (1995): Improved assessment of significant activation in functional magnetic resonance imaging (fMRI): Use of a cluster-size threshold. Magn Reson Med 33:636–647.

Fox PT, Narayana S, Tandon N, Sandoval H, Fox SP, Kochunov P, Lancaster JL (2004): Column-based model of electric field excitation of cerebral cortex. Hum Brain Mapp 22:1–14.

Frahm J, Merboldt KD, Hanicke W, Kleinschmidt A, Boecker H (1994): Brain or vein—oxygenation or flow? On signal physiology in functional MRI of human brain activation. NMR Biomed 7:45–53.

Friston KJ, Worsley KJ, Frackowiak RSJ, Mazziotta JC, Evans AC (1994): Assessing the significance of focal activations using their spatial extent. Hum Brain Mapp 1:210–220.

Geyer S, Ledberg A, Schleicher A, Kinomura S, Schormann T, Burgel U, Klingberg T, Larsson J, Zilles K, Roland PE (1996): Two different areas within the primary motor cortex of man. Nature 382:805–807.

Grefkes C, Eickhoff SB, Nowak DA, Dafotakis M, Fink GR (2008): Dynamic intra- and interhemispheric interactions during unilateral and bilateral hand movements assessed with fMRI and DCM. Neuroimage 41:1382–1394.

Goense JB, Logothetis NK (2006): Laminar specificity in monkey V1 using high-resolution SE-fMRI. Magn Reson Imaging 24: 381–392.

Harel N, Lin J, Moeller S, Ugurbil K, Yacoub E (2006): Combined imaging-histological study of cortical laminar specificity of fMRI signals. Neuroimage 29:879–887.

Herbsman T, Forster L, Molnar C, Dougherty R, Christie D, Koola J, Ramsey D, Morgan PS, Bohning DE, George MS, Nahas Z (2009): Motor threshold in transcranial magnetic stimulation: The impact of white matter fiber orientation and skull-to-cortex distance. Hum Brain Mapp 30:2044–2055.

Herwig U, Kolbel K, Wunderlich AP, Thielscher A, von Tiesenhausen C, Spitzer M, Schonfeldt-Lecuona C (2002): Spatial congruence of neuronavigated transcranial magnetic stimulation and functional neuroimaging. Clin Neurophysiol 113:462–468.

Hess CW, Mills KR, Murray NM (1987): Responses in small hand muscles from magnetic stimulation of the human brain. J Physiol 388:397–419.

Jenkinson M, Bannister P, Brady M, Smith S (2002): Improved optimization for the robust and accurate linear registration and motion correction of brain images. Neuroimage 17:825–841.

Jenkinson M, Smith S (2001): A global optimisation method for robust affine registration of brain images. Med Image Anal 5: 143–156.

Kennan RP, Zhong J, Gore JC (1994): Intravascular susceptibility contrast mechanisms in tissues. Magn Reson Med 31:9–21.

Kim SG, Tsekos NV, Ashe J (1997): Multi-slice perfusion-based functional MRI using the FAIR technique: Comparison of CBF and BOLD effects. NMR Biomed 10:191–196.

Kozel FA, Nahas Z, deBrux C, Molloy M, Lorberbaum JP, Bohning D, Risch SC, George MS (2000): How coil–cortex distance relates to age, motor threshold, and antidepressant response to repetitive transcranial magnetic stimulation. J Neuropsychiatry Clin Neurosci 12:376–384.

Krings T, Buchbinder BR, Butler WE, Chiappa KH, Jiang HJ, Cosgrove GR, Rosen BR (1997): Functional magnetic resonance imaging and transcranial magnetic stimulation: Complementary approaches in the evaluation of cortical motor function. Neurology 48:1406–1416.

Lee SP, Silva AC, Kim SG (2002): Comparison of diffusion-weighted high-resolution CBF and spin-echo BOLD fMRI at 9.4 T. Magn Reson Med 47:736–741.

Lewko JP, Stokić DS, Tarkka IM (1996): Dissociation of cortical areas responsible for evoking excitatory and inhibitory responses in the small hand muscles. Brain Topogr 8:397–405.

Liu TT, Brown GG (2007): Measurement of cerebral perfusion with arterial spin labeling: Part 1. Methods. J Int Neuropsychol Soc 13:517–525.

Logothetis NK (2008): What we can do and what we cannot do with fMRI? Nature 453:869–878.

Lotze M, Kaethner RJ, Erb M, Cohen LG, Grodd W, Topka H (2003): Comparison of representational maps using functional magnetic resonance imaging and transcranial magnetic stimulation. Clin Neurophysiol 114:306–312.

Luh WM, Wong EC, Bandettini PA, Hyde JS (1999): QUIPSS II with thin-slice TI1 periodic saturation: A method for improving accuracy of quantitative perfusion imaging using pulsed arterial spin labeling. Magn Reson Med 41:1246–1254.

Luh WM, Wong EC, Bandettini PA, Ward BD, Hyde JS (2000): Comparison of simultaneously measured perfusion and BOLD signal increases during brain activation with T(1)-based tissue identification. Magn Reson Med 44:137–143.

Maccabee PJ, Amassian VE, Eberle LP, Cracco RQ (1993): Magnetic coil stimulation of straight and bent amphibian and mammalian peripheral nerve in vitro: Locus of excitation. J Physiol 460:201–219.

Mills KR, Boniface SJ, Schubert M (1992): Magnetic brain stimulation with a double coil: The importance of coil orientation. Electroencephalogr Clin Neurophysiol 85:17–21.

Norris DG (2003): High field human imaging. J Magn Reson Imaging 18:519–529.

Norris DG, Zysset S, Mildner T, Wiggins CJ (2002): An investigation of the value of spin-echo-based fMRI using a Stroop color-word matching task and EPI at 3 T. Neuroimage 15: 719–726.

Oja JM, Gillen J, Kauppinen RA, Kraut M, van Zijl PC (1999): Venous blood effects in spin-echo fMRI of human brain. Magn Reson Med 42:617–626.

Oldfield RC (1971): The assessment and analysis of handedness: The Edinburgh inventory. Neuropsychologia 9:97–113.

Rothwell JC, Thompson PD, Day BL, Boyd S, Marsden CD (1991): Stimulation of the human motor cortex through the scalp. Exp Physiol 76:159–200.

Salinas FS, Lancaster JL, Fox PT (2009): 3D modeling of the total electric field induced by transcranial magnetic stimulation using the boundary element method. Phys Med Biol 54:3631–3647.

Sanes JN, Donoghue JP (2000): Plasticity and primary motor cortex. Annu Rev Neurosci 23:393–415.

Schmahmann JD, Pandya DN (2006): Fiber Pathways of the Brain. Oxford: Oxford University Press, 654 p.

Silva AC (2005): Perfusion-based fMRI: Insights from animal models. J Magn Reson Imaging 22:745–750.

Silva AC, Williams DS, Koretsky AP (1997): Evidence for the exchange of arterial spin-labeled water with tissue water in rat brain from diffusion-sensitized measurements of perfusion. Magn Reson Med 38:232–237.

Smith SM (2002): Fast robust automated brain extraction. Hum Brain Mapp 17:143–155.

Sparing R, Buelte D, Meister IG, Paus T, Fink GR (2008): Transcranial magnetic stimulation and the challenge of coil placement: A comparison of conventional and stereotaxic neuronavigational strategies. Hum Brain Mapp 29:82–96.

Terao Y, Ugawa Y, Sakai K, Miyauchi S, Fukuda H, Sasaki Y, Takino R, Hanajima R, Furubayashi T, Putz B, Kanazawa I (1998): Localizing the site of magnetic brain stimulation by functional MRI. Exp Brain Res 121:145–152.

Thielscher A, Wichmann FA (2009): Determining the cortical target of transcranial magnetic stimulation. Neuroimage 47:1319–1330.

Thulborn KR, Chang SY, Shen GX, Voyvodic JT (1997): High-resolution echo-planar fMRI of human visual cortex at 3.0 Tesla. NMR Biomed 10:183–190.

Tjandra T, Brooks JC, Figueiredo P, Wise R, Matthews PM, Tracey I (2005): Quantitative assessment of the reproducibility of functional activation measured with BOLD and MR perfusion imaging: Implications for clinical trial design. Neuroimage 27: 393–401.

Uludag K, Muller-Bierl B, Ugurbil K (2009): An integrative model for neuronal activity-induced signal changes for gradient and spin echo functional imaging. Neuroimage 48:150–165.

Walsh V, Cowey A (2000): Transcranial magnetic stimulation and cognitive neuroscience. Nat Rev Neurosci 1:73–79.

Wassermann EM (1998): Risk and safety of repetitive transcranial magnetic stimulation: Report and suggested guidelines from the International Workshop on the Safety of Repetitive Transcranial Magnetic Stimulation, June 5–7, 1996. Electroencephalogr Clin Neurophysiol 108:1–16.

Wassermann EM, Wang B, Zeffiro TA, Sadato N, Pascual-Leone A, Toro C, Hallett M (1996): Locating the motor cortex on the MRI with transcranial magnetic stimulation and PET. Neuroimage 3:1–9.

Wilson SA, Thickbroom GW, Mastaglia FL (1995): Comparison of the magnetically mapped corticomotor representation of a muscle at rest and during low-level voluntary contraction. Electroencephalogr Clin Neurophysiol 97:246–250.

Woolrich MW, Ripley BD, Brady M, Smith SM (2001): Temporal autocorrelation in univariate linear modeling of FMRI data. Neuroimage 14:1370–1386.

Worsley KJ, Evans AC, Marrett S, Neelin P (1992): A three-dimensional statistical analysis for CBF activation studies in human brain. J Cereb Blood Flow Metab 12:900–918.

Ye Y, Zhuo Y, Xue R, Zhou XJ (2009): BOLD fMRI using a modified HASTE sequence. Neuroimage 49:457–466.

Yousry TA, Schmid UD, Alkadhi H, Schmidt D, Peraud A, Buettner A, Winkler P (1997): Localization of the motor hand area to a knob on the precentral gyrus. A new landmark. Brain 120 (Pt 1):141–157.

Zappe AC, Pfeuffer J, Merkle H, Logothetis NK, Goense JB (2008): The effect of labeling parameters on perfusion-based fMRI in nonhuman primates. J Cereb Blood Flow Metab 28:640–652.